J. Fluid Mech. (2020), *vol.* 885, R1, doi:10.1017/jfm.2019.992

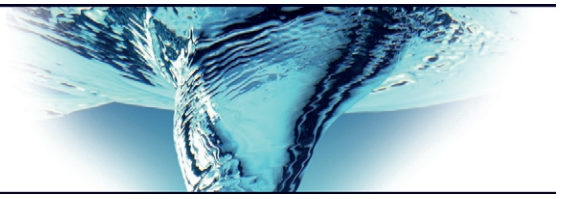

JFM RAPIDS
journals.cambridge.org/rapids

Resolvent analysis on the origin of two-dimensional transonic buffet

Yoimi Kojima[1,†], **Chi-An Yeh**[2], **Kunihiko Taira**[2] **and Masaharu Kameda**[1]

[1]Department of Mechanical Systems Engineering, Tokyo University of Agriculture and Technology, Koganei, Tokyo, 184-8588, Japan

[2]Department of Mechanical and Aerospace Engineering, University of California, Los Angeles, CA 90095, USA

(Received 9 October 2019; revised 8 November 2019; accepted 17 November 2019)

Resolvent analysis is performed to identify the origin of two-dimensional transonic buffet over an airfoil. The base flow for the resolvent analysis is the time-averaged flow over a NACA 0012 airfoil at a chord-based Reynolds number of 2000 and a free-stream Mach number of 0.85. We reveal that the mechanism of buffet is buried underneath the global low-Reynolds-number flow physics. At this low Reynolds number, the dominant flow feature is the von Kármán shedding. However, we show that with the appropriate forcing input, buffet can appear even at a Reynolds number that is much lower than what is traditionally associated with transonic buffet. The source of buffet is identified to be at the shock foot from the windowed resolvent analysis, which is validated by companion simulations using sustained forcing inputs based on resolvent modes. We also comment on the role of perturbations in the vicinity of the trailing edge. The present study not only provides insights on the origin of buffet but also serves a building block for low-Reynolds-number compressible aerodynamics in light of the growing interests in Martian flights.

Key words: high-speed flow, shock waves

1. Introduction

Transonic flow over an airfoil exhibits complex dynamics from the interplay among the unsteady shock motion, flow separation due to the shock/boundary layer interaction, and the generation and propagation of pressure waves. Under certain ranges of angle of attack and Mach number, the shock wave oscillates vigorously, creating a highly unsteady flow (Lee 2001). This shock-wave oscillation phenomenon, known as transonic buffet, is caused by a self-sustaining aerodynamic instability. The large-scale motion of the shock induces violent fluctuations in aerodynamic forces and leads to structural vibrations. The level of unsteadiness induced by transonic

† Email address for correspondence: y-kojima@st.go.tuat.ac.jp

buffet can be so large that it can compromise the integrity of aircraft structure and flight safety. For these reasons, transonic buffet is a major limiting factor for aircraft flight envelopes and has been the focus of many studies, as summarized recently by Giannelis, Vio & Levinski (2017).

Various experimental and numerical studies have been devoted to the characterization of transonic buffet. Past studies have revealed that the typical oscillating frequency of shock waves is very low, with the chord-based Strouhal number being approximately 0.06 (Deck 2005; Jacquin *et al.* 2009). This low frequency is distinguished from other unsteady phenomena around the airfoil related to the velocity fluctuations in the separation region and vortex shedding in the wake (Sartor, Mettot & Sipp 2014). More recently, some researchers have reported that a transonic buffet on a three-dimensional wing has spanwise instability with a much higher frequency, where $0.2 < St < 0.6$ (Dandois 2016; Ohmichi, Ishida & Hashimoto 2018).

Separation on the airfoil induced by shock-wave/boundary layer interaction (SWBLI) plays an important role in transonic buffet. Early experiments (Levy 1978; Seegmiller, Marvin & Levy Jr. 1978) showed that the onset of shock oscillation occurred when the separation generated at the shock foot reaches the trailing edge of the airfoil. Recent numerical studies (Iovnovich & Raveh 2012; Grossi, Braza & Hoarau 2014; Fukushima & Kawai 2018) reported that unsteadiness of the separation is closely tied to buffet. When the shock moves downstream from its upstream position, the shock becomes weaker and the flow behind the shock remains attached. In contrast, when the shock moves upstream from its downstream location, the shock becomes stronger, and causes large-scale separation.

A number of studies have analysed the self-sustained mechanism of shock-wave oscillation. Lee (2001) argued that the pressure wave propagating between the shock wave and the trailing edge of the airfoil plays a critical role in feedback to maintain shock oscillation. More recently, global linear stability analysis performed by Crouch *et al.* (2009) extracted the growth rate of the buffet fluctuation with respect to the time-averaged flow field based on the eigenvalue problem of a linearized Navier–Stokes operator. They examined the linear stability of transonic flow around a two-dimensional NACA 0012 airfoil obtained from Reynolds-averaged Navier–Stokes (RANS) simulations. Analysing the critical angle of attack and Mach number of the buffet onset, the critical values agreed reasonably with the experimental results obtained by McDevitt & Okuno (1985). Nonetheless, the origin of the transonic buffet is still under debate, with open questions on the validity of the linear stability formalism for base flows that are not the exact solution of the Navier–Stokes equations.

Recently, Sartor *et al.* (2014) employed global stability, adjoint, and resolvent analysis to examine transonic buffet flow around a NACA 0012 airfoil at $Re = 3 \times 10^6$. At the buffet frequency, they used resolvent analysis to find that the essential origin of shock unsteadiness is at the shock foot region on the suction side of the airfoil. There are also reports, including Nitzsche (2009), that identified various sources that can trigger buffet, such as the motion of flaps, pitch oscillation, and translation of the airfoil. Based on these observations, various methods have been developed to control buffet, including vortex generators (McCormick 1993) and trailing-edge deflection techniques (Gao *et al.* 2017).

The objective of the present study is to systematically determine the origin of two-dimensional transonic buffet flow around a NACA 0012 airfoil at a low Reynolds number of $Re = 2000$ in the absence of any modelling terms. We reveal the input–output relationship for transonic buffet with the resolvent analysis, which

can extract not only the frequency response but also identify the forcing (input) and response (output) modes of flow systems (Trefethen *et al.* 1993; Jovanović & Bamieh 2005; McKeon & Sharma 2010; Taira *et al.* 2017, 2019; Yeh & Taira 2019). To validate that the identified source of buffet is indeed the driving mechanism for sustained oscillations, we perform direct numerical simulations (DNS) to show that buffet can appear even in low-Reynolds-number flows under appropriate conditions. This analysis not only provides the fundamental insights into transonic buffet but also serves as a building block for low-Reynolds-number compressible aerodynamics ($Re \approx O(10^3$–$10^5)$). This area of aerodynamics has traditionally been overlooked but is now becoming important for developing high-efficiency wings and propulsion systems for unmanned aircraft on Mars (Anyoji *et al.* 2015; Munday *et al.* 2015; Koning, Johnson & Grip 2019).

We discuss the problem description, simulation approach and resolvent analysis in § 2. The insights gained from resolvent analysis are offered in § 3 with discussions on the source of buffet. Our findings are validated by forcing the flow at the identified source to stimulate the emergence of buffet. Finally, we offer concluding remarks in § 4.

2. Problem set-up

2.1. *Problem description*

We consider two-dimensional laminar transonic flows over a NACA 0012 airfoil at a free-stream Mach number $M_\infty \equiv U_\infty/a_\infty = 0.85$, a chord-based Reynolds number of $Re_{L_c} \equiv U_\infty L_c/\nu_\infty = 2000$ and an angle of attack of $\alpha = 3°$. Here, U_∞ is the free-stream velocity, a_∞ is the free-stream sonic speed, L_c is the chord length and ν_∞ is the free-stream kinetic viscosity. The Prandtl number is set to $Pr = 0.7$. While not reported, we also considered $\alpha = 1°$ and $5°$. As we obtained analogous results for these angles of attack, we present only the representative case of $\alpha = 3°$ herein. Shock waves form around the airfoil under these conditions, making this base flow an appropriate candidate for this study.

2.2. *Flow simulation*

We simulate transonic flows over the airfoil by solving the compressible Navier–Stokes equations in a two-dimensional setting using the finite-volume solver CharLES, which is second-order accurate in space and third-order accurate in time (Brès *et al.* 2017). We employ a second-order fully unstructured essentially non-oscillatory (ENO) method (Shi, Hu & Shu 2002) for shock capturing. A C-shaped hexahedral mesh is used for the simulations, as shown in figure 1. The computational domain has an extent of $x_c/L_c \in [-50, 50]$ and $y_c/L_c \in [-50, 50]$, where x_c and y_c represent the chordwise and chord-normal directions, respectively. The airfoil is positioned with its leading edge at the origin. The domain is discretized into 70 000 cells with 100 nodes on each side of the airfoil, 90 nodes along the wake and 80 nodes in the normal direction, where the minimum wall-adjacent Δy is set to be $\Delta y/L_c = 1.42 \times 10^{-3}$. A grid convergence study has been conducted with respect to the time-averaged flow to ensure sufficient spatial resolution for this computational grid. At the far-field boundary, the free-stream condition is prescribed as $[\rho, v_{x_c}, v_{y_c}, T] = [\rho_\infty, U_\infty \cos\alpha, U_\infty \sin\alpha, T_\infty]$, where ρ is density and T is temperature. The free-stream angle is changed through the prescription of the far-field flow velocities v_{x_c} and v_{y_c} in the x_c and y_c directions, respectively. A no-slip adiabatic condition is prescribed over the airfoil. Along the outlet boundary, a sponge layer (Freund 1997) is applied over $x_c/L_c \in [40, 50]$, with the target state being the running-averaged flow over $tU_\infty/L_c = 1$. The time integration is performed at a constant Courant–Friedrichs–Lewy number of 1.

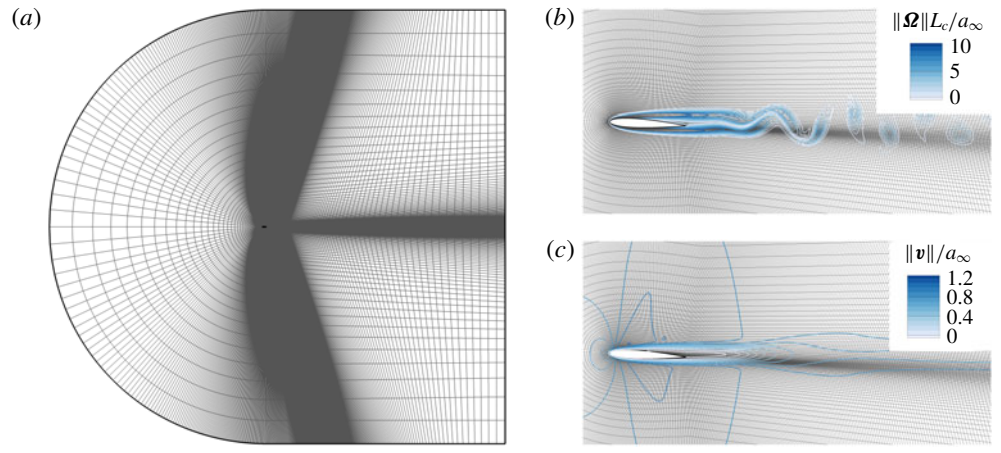

FIGURE 1. The computational grid used for numerical simulation and resolvent analysis. (*a*) The whole computational domain. The enlarged views around the airfoil are shown with the (*b*) instantaneous magnitude of normalized vorticity and (*c*) time-averaged velocity fields.

2.3. *Resolvent analysis*

The objective of the present study is to reveal the input–output relationship for two-dimensional transonic buffet and identify the origin of the energetic shock-wave oscillations. In this study, we focus our resolvent analysis on two-dimensional modes, which are essential in all buffet phenomena (Iovnovich & Raveh 2012; Sartor *et al.* 2014; Ohmichi *et al.* 2018). Note that resolvent analysis itself is not limited to two-dimensional flow. Further resolvent analysis of transonic buffet over three-dimensional wings could extract the spanwise modes, which have been reported in previous studies (Iovnovich & Raveh 2015; Ohmichi *et al.* 2018).

We consider the Reynolds decomposition of the flow variable $\boldsymbol{q}(\boldsymbol{x}, t) = [\rho, v_x, v_y, T]$ into the sum of a time-averaged base state $\bar{\boldsymbol{q}}(\boldsymbol{x})$ and the statistically stationary fluctuating component $\boldsymbol{q}'(\boldsymbol{x}, t)$, which enables us to express the Navier–Stokes equation as

$$\partial_t \boldsymbol{q}' = \boldsymbol{L}_{\bar{q}} \boldsymbol{q}' + \boldsymbol{B}\boldsymbol{f}', \tag{2.1}$$

where $\boldsymbol{L}_{\bar{q}}$ is the linearized Navier–Stokes operator about the mean flow $\bar{\boldsymbol{q}}$ (McKeon & Sharma 2010) and $\boldsymbol{B}$ is an input matrix that can spatially window the forcing input $\boldsymbol{f}'$. We construct the discrete linear operator $\boldsymbol{L}_{\bar{q}}$, incorporating the boundary conditions of $[\rho', v'_{x_c}, v'_{y_c}, \nabla_n T'] = 0$ over the airfoil and the far field, and $\nabla_n[\rho', v'_{x_c}, v'_{y_c}, T'] = 0$ at the computational outlet, where ∇_n denotes the surface-normal gradient. The spatial discretization for $\boldsymbol{L}_{\bar{q}}$ is performed on the same mesh used in the flow simulation, as shown in figure 1. When the time-averaged flow is chosen as the base state in resolvent analysis, the finite-amplitude nonlinear terms with respect to $\boldsymbol{q}'$ are incorporated in $\boldsymbol{f}'$, which can be interpreted as a sustained forcing input within the natural feedback system (McKeon & Sharma 2010). Moreover, we consider an observable output vector $\boldsymbol{y}$ given by $\boldsymbol{y} = \boldsymbol{C}\boldsymbol{q}'$, such that spatial windowing $\boldsymbol{C}$ can be applied in general (Jeun, Nichols & Jovanović 2016; Schmidt *et al.* 2018).

With the Fourier representation $\boldsymbol{q}'(\boldsymbol{x}, t) = \int_{-\infty}^{\infty} \hat{\boldsymbol{q}}_\omega(\boldsymbol{x}) \mathrm{e}^{-\mathrm{i}\omega t}\, \mathrm{d}\omega$, equation (2.1) can be expressed in frequency space as

$$-\mathrm{i}\omega \hat{\boldsymbol{q}}_\omega = \boldsymbol{L}_{\bar{q}} \hat{\boldsymbol{q}}_\omega + \boldsymbol{B}\hat{\boldsymbol{f}}_\omega, \quad \text{with } \hat{\boldsymbol{y}}_\omega = \boldsymbol{C}\hat{\boldsymbol{q}}_\omega. \tag{2.2}$$

The input–output relationship between the input (forcing) $\hat{\boldsymbol{f}}_\omega$ and the output (response) $\hat{\boldsymbol{y}}_\omega$ at a specified frequency ω becomes

$$\hat{\boldsymbol{y}}_\omega = \boldsymbol{R}_{\bar{\boldsymbol{q}}}(\omega)\hat{\boldsymbol{f}}_\omega, \quad \text{where } \boldsymbol{R}_{\bar{\boldsymbol{q}}}(\omega) = \boldsymbol{C}[-\mathrm{i}\omega\boldsymbol{I} - \boldsymbol{L}_{\bar{\boldsymbol{q}}}]^{-1}\boldsymbol{B}. \tag{2.3}$$

Here, $\boldsymbol{R}_{\bar{\boldsymbol{q}}}(\omega)$ is referred to as the resolvent (operator). It serves as a transfer function that amplifies (or attenuates) the harmonic forcing input $\hat{\boldsymbol{f}}_\omega$ and maps it to the response $\hat{\boldsymbol{y}}_\omega$. In this study, the base flows are found to be stable according the eigenvalues of the linear operators $\boldsymbol{L}_{\bar{\boldsymbol{q}}}$. Therefore, we consider a real-valued frequency ω in constructing $\boldsymbol{R}_{\bar{\boldsymbol{q}}}(\omega)$ for our resolvent analysis (Jovanović 2004; Yeh & Taira 2019).

Resolvent analysis identifies the dominant directions along which $\hat{\boldsymbol{f}}_\omega$ can be most amplified through $\boldsymbol{R}_{\bar{\boldsymbol{q}}}(\omega)$ to form the corresponding response $\hat{\boldsymbol{y}}_\omega$. This is accomplished by performing the singular value decomposition (SVD) of the resolvent

$$\boldsymbol{R}_{\bar{\boldsymbol{q}}}(\omega) = \boldsymbol{Y}\boldsymbol{\Sigma}\boldsymbol{F}^*, \tag{2.4}$$

where $\boldsymbol{F}^*$ denotes the Hermitian of $\boldsymbol{F}$. Resolvent analysis interprets left and right singular vectors $\boldsymbol{Y} = [\hat{\boldsymbol{y}}_1, \hat{\boldsymbol{y}}_2, \ldots, \hat{\boldsymbol{y}}_m]$ and $\boldsymbol{F} = [\hat{\boldsymbol{f}}_1, \hat{\boldsymbol{f}}_2, \ldots, \hat{\boldsymbol{f}}_m]$, respectively, as response modes and forcing modes, with the magnitude-ranked singular values $\boldsymbol{\Sigma} = \mathrm{diag}(\sigma_1, \sigma_2, \ldots, \sigma_m)$ being the amplification (gain) for the corresponding forcing–response pair at frequency ω. We examine the modal structures of the dominant forcing and response modes $[\hat{\boldsymbol{f}}_1, \hat{\boldsymbol{y}}_1]$ to study the origin of transonic buffet over this canonical airfoil.

The application of a spatial window to the global response $\hat{\boldsymbol{q}}_\omega$ can be implemented by specifying $\boldsymbol{C}$ as a diagonal weight matrix with unit weights inside the window and zeros otherwise. This window is chosen to highlight the location over the suction surface where oscillatory motion of the shock wave appears and then limits the output to be within inside of window, as is illustrated in figure 3. While matrix $\boldsymbol{B}$ for forcing can be designed in a similar manner, we use $\boldsymbol{B} = \boldsymbol{I}$ such that there is no restriction on the region of forcing to identify the source of buffet. The use of window $\boldsymbol{C}$ in the resolvent analysis can help reveal the optimal energy amplification from forcing to a local response in the shock region over the suction surface of the airfoil.

3. Results

3.1. *Base flow*

We simulate the unsteady two-dimensional flow over a NACA 0012 airfoil at $\alpha = 3^\circ$ for $M_\infty = 0.85$ and $Re_{L_c} = 2000$. An instantaneous vorticity field from DNS is shown in figure 2(*a*). The laminar vortex sheets generated from the pressure and suction sides of the wing roll into vortices in the wake. This representative transonic flow at low Reynolds number exhibits a distinct shedding frequency of $St \equiv fL_c/U_\infty = 1.0$. This frequency can be detected from the power spectral density (PSD) of the velocity probe at $(x, y)/L_c = (2.10, -0.11)$, along with its harmonics, in figure 2(*b*). For this flow, we do not directly observe buffet over the airfoil. Nitzsche (2009) investigated the frequency response of shock waves to small perturbations and found that the external forcing to transonic flow around an airfoil can trigger shock-wave oscillations even if the base flow is stable. He has reported that the maximum gain was observed close to the buffet onset angle. The present resolvent analysis holds great potential to reveal the optimal input–output relationship with respect to the onset of buffet.

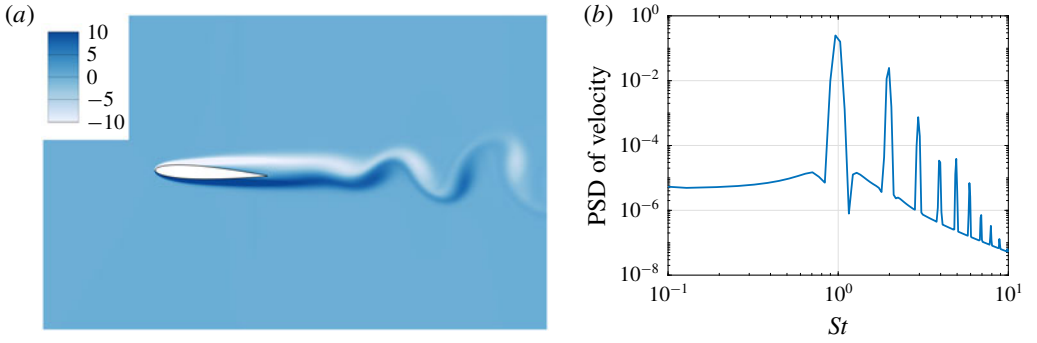

FIGURE 2. Unsteady transonic flow over a NACA 0012 airfoil. (*a*) Instantaneous vorticity field ($\Omega_z L_c/a_\infty$). (*b*) Power spectral density of v_y/a_∞ probed at $(x, y)/L_c = (2.10, -0.11)$.

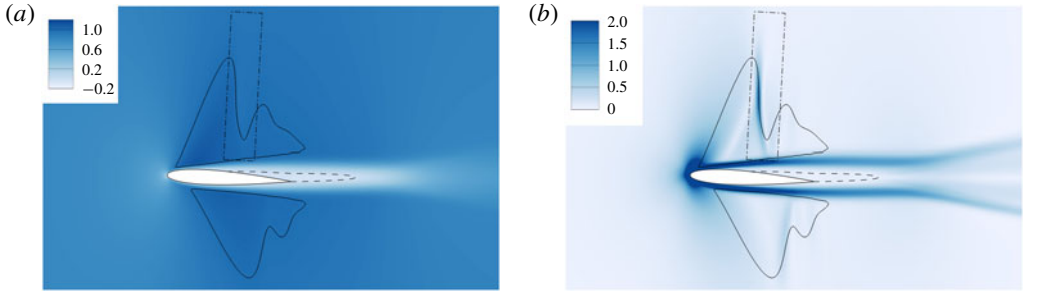

FIGURE 3. Time-averaged flow field around the NACA 0012 airfoil. (*a*) Streamwise velocity (v_x/a_∞). (*b*) Numerical schlieren with density gradient magnitude ($\|\nabla\rho\|L_c/\rho_\infty$). Regions enclosed by the solid and broken curves represent the supersonic and recirculation regions, respectively. The dashed-dotted box depicts the spatial window for the filtered resolvent analysis.

To perform resolvent analysis, we consider the time-averaged flow to be the base state. The temporal averaging is performed over $tU_\infty/L_c \in [0, 350]$ to ensure statistical convergence. This long window for averaging allows us to set the minimum frequency in the resolvent analysis at 2.9×10^{-3}, which is sufficiently small compared with the dominant buffet frequency of $St \approx 0.07$ (Jacquin *et al.* 2009; Sartor *et al.* 2014). The time-averaged streamwise velocity and the numerical schlieren fields are shown in figure 3. The solid and broken curves in figures 3(*a*) and 3(*b*) indicate the contour lines for $M = 1$ and $v_x = 0$, respectively. The area enclosed in the solid curve corresponds to the supersonic region, while the region surrounded by the broken curves represents the separated flow region. Weak shock waves are observed in the supersonic regions. The supersonic region on the suction side is further divided into two stages of acceleration–deceleration phases according to the λ-type structure of the shock waves (Delery 1985). The first stage corresponds to the initial flow acceleration near the leading edge. The flow surpasses the sonic speed and decelerates after the first shock wave. Over the airfoil, the flow undergoes the second stage of acceleration and forms the second shock structure near the trailing edge. Strong inverse pressure gradients due to λ-type shock waves are observed aft of the first acceleration.

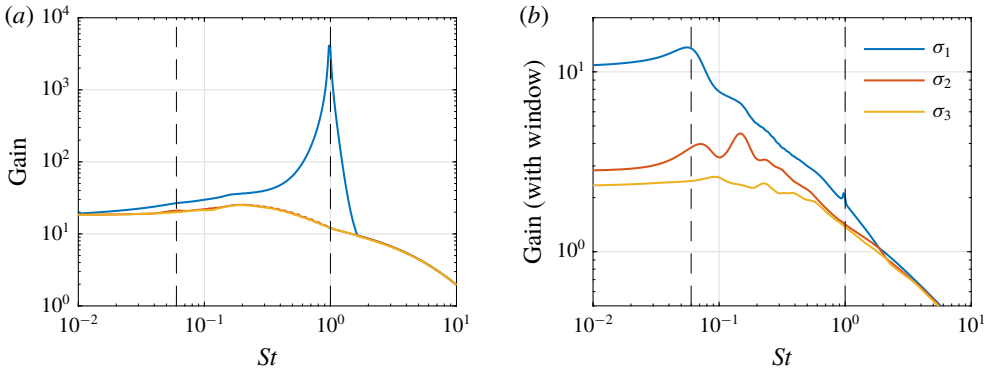

FIGURE 4. (*a*) Original and (*b*) windowed resolvent gains over St.

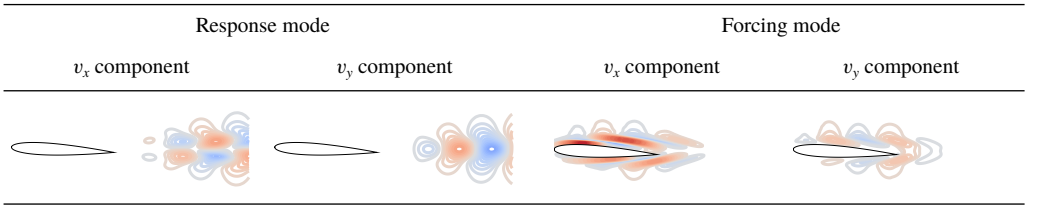

FIGURE 5. Response and forcing modes normalized by the velocity magnitude for $St = 1$.

3.2. *Resolvent analysis*

As transonic buffet is characterized by the energetic shock-wave oscillation over the airfoil, the cause of buffet may be uncovered by closely studying the input–output process at the relevant fluctuation frequency using the resolvent analysis described in § 2.3. Let us first present in figure 4(*a*) the distribution of the leading gain σ_1 over a range of frequencies from resolvent analysis without windowing. The leading gain σ_1 shows a distinct peak at $St = 1$ corresponding to the von Kármán shedding frequency. However, there are no other distinct peaks appearing in the gain distribution for σ_1. This is expected since the dominant physics for this low-Reynolds-number base flow is the wake shedding. We do not observe noticeable peaks even for subdominant modes.

Let us present the dominant resolvent modes for $St = 1$ without windowing. Since the gain peaks at the shedding frequency, response modes exhibit modal shapes that are representative of convective dynamics in the wake, as visualized in figure 5. The forcing modes are present in the vicinity of the airfoil where shear is large, as can be observed from figure 3. This is in line with our understanding of the formation of wake vortices from the roll up of shear layers. These observations are also in agreement with modal analysis for subsonic flows over airfoils (Zhang & Samtaney 2016; Yeh & Taira 2019).

Next, let us consider the gain distribution from the windowed resolvent analysis. Here, the output is windowed by operator $\boldsymbol{C}$ with a spatial profile that is restricted to the region in the vicinity of the shock, as shown in figure 3. With the output of resolvent analysis focusing on the fluctuations close to the standing shock, we find that the dominant gain σ_1 shows a peak at the buffet frequency of $St = 0.06$, which is in agreement with past numerical and experimental findings (Deck 2005; Jacquin *et al.* 2009; Sartor *et al.* 2014; Dandois 2016), which were conducted at high Reynolds

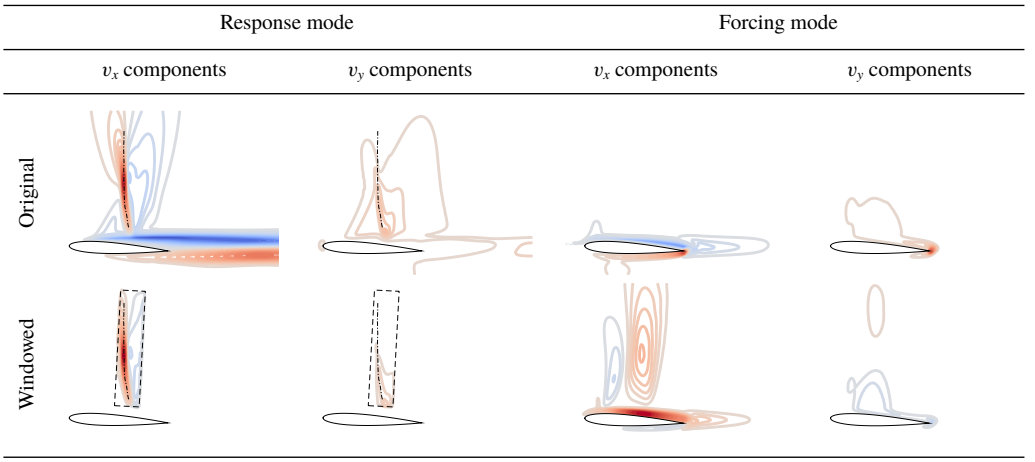

FIGURE 6. The original (top) and the windowed (bottom) resolvent modes normalized by the velocity magnitude for $St = 0.06$. The dashed-dotted lines depicts the position of the shock on the suction side.

numbers of $Re_{L_c} > O(10^6)$. For subdominant gains, we observe peaks appearing at superharmonics that capture smaller-scale oscillations. We can observe a minor peak in σ_1 at $St = 1$. However, the overall amplification process for the shock region is focused towards the low-frequency components at the buffet frequency. This suggests that the amplification physics for buffet is buried underneath the global input–output dynamics at this low Reynolds number. We also note that the conclusive assessment on the buffet physics is robust against the choice of the response window. A prominent peak at the buffet frequency $St = 0.06$ with similar forcing structure is still revealed using a different window that covers the entire suction surface over $x_c \in [0, 1]$ and $y_c \in [0, \infty)$.

We visualize the response and forcing modes that correspond to the buffet frequency of $St = 0.06$ as identified from the gain distribution with windowed resolvent analysis. These modes in figure 6 are quite different from the modes at $St = 1$. While the response modes for $St = 1$ exhibit convective oscillations in the wake region, the response modes for $St = 0.06$ are predominantly supported in the region of the standing shock. The windowed analysis is able to highlight the response in the region of the shock. For these reasons, the response modes can be seen as the oscillatory mechanism for buffet.

The input to generate the buffet unsteadiness can be identified by studying the forcing modes. We can observe from figure 6 that the forcing modes from both resolvent analysis with and without windowing show the boundary layer around the airfoil to be the source of buffet. In particular, from the windowed forcing mode, we find that the region corresponding to the shock foot is the most sensitive region to instigate the buffet phenomenon – which is in agreement with Sartor *et al.* (2014), who have carried out resolvent analysis at $Re = 3 \times 10^6$. In a number of past studies (Deck 2005; Grossi *et al.* 2014; Fukushima & Kawai 2018), the SWBLI at the shock foot exhibited turbulent boundary layer separation, which was suspected to play a role in the emergence of buffet. The current result by the windowed resolvent analysis suggests that the low-frequency buffet can be stimulated even though the boundary layer is entirely laminar at a significantly lower Reynolds number of

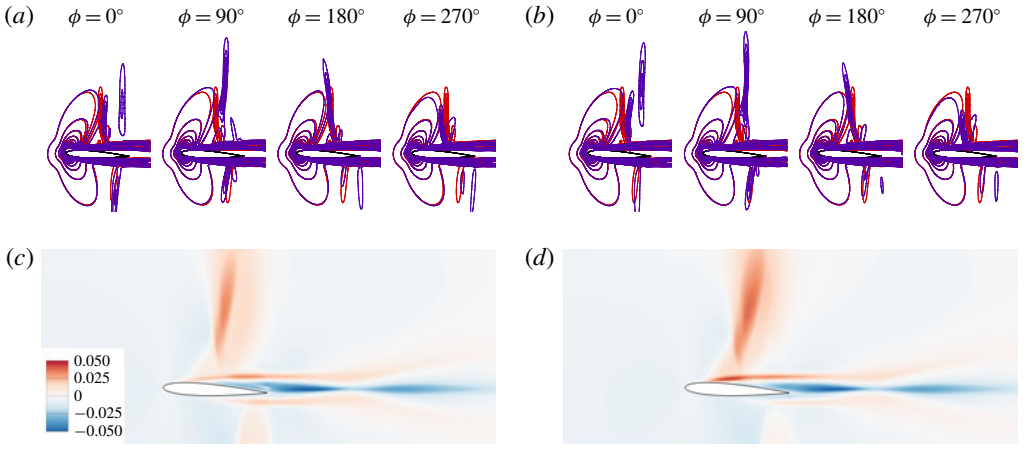

FIGURE 7. Transonic flows over the airfoil with perturbations added in the form of the dominant forcing modes from original (*a*,*c*) and windowed resolvent analysis (*b*,*d*). The motions of the shock wave are visualized in (*a*,*b*) with the blue contour lines in four phases ϕ_f with respect to the forced buffet cycle, on top of the red lines for the unforced case. Both contour lines display levels of $\|\nabla\rho\|L_c/\rho_\infty$. Visualized in (*c*,*d*) are differences of the r.m.s. of streamwise velocity fields $\Delta v_{rms,x}/a_\infty$, where $\Delta v_{rms,x} \equiv v_{rms,x,forced} - v_{rms,x,unforced}$.

$Re = 1000$. Interestingly, the response modes do not show fluctuations about the weaker pressure-side shock wave observed in the numerical schlieren of figure 3(*b*).

Let us also bring attention to the vicinity of the trailing edge for the original forcing modes in figure 6. We can observe that there is a compact region at the trailing edge that appears in the original forcing modes. Since the dominant response mode covers the wing surface, its fluctuation alters the circulation of the airfoil, making the trailing edge act as sensitive location due to its singular nature from the cusp geometry. For this reason, we see the trailing edge also supporting the fluctuations in the original forcing mode. This observation is in tune with the report of Nitzsche (2009) and past control techniques using a trailing-edge deflector to effectively attenuate buffet (Gao *et al.* 2017). The blockage of flow around the trailing edge by the deflector can obstruct the change in circulation in a kinematic manner. The current resolvent analysis with windowing is able to identify these sources of buffet in a clear manner. While the present discussion is concerned only with $\alpha = 3°$, we note that similar observations are made for other angles of attack of $\alpha = 1°$ and $5°$.

To corroborate our findings from resolvent analysis, we perform companion simulations of transonic flows over the airfoil with perturbations added in the shape of forcing modes. We add the forcing to the flow as a body force, $\boldsymbol{f}_{body}$, with the spatial profiles given by the dominant forcing modes at $St = 0.06$ (see figure 6). The amplitude of forcing is chosen such that the momentum coefficient $C_\mu \equiv \|\boldsymbol{f}_{body}\|/(\frac{1}{2}\rho_\infty U_\infty^2 L_c) = 0.003$, which is low for this viscous flow problem (Munday & Taira 2018). These perturbations with the spatial profiles of the primary forcing modes without and with windowing do indeed stimulate the emergence of buffet over the airfoil, as shown in figure 7(*a*,*b*). Even at this low Reynolds number, the standing shock is found to oscillate violently with large-amplitude motion over the airfoil. The amplification in the oscillation from the forcing input to the flow response (including nonlinear effects) is assessed using $\Gamma = \kappa\Delta\|\boldsymbol{u}_{rms}\|/\|\boldsymbol{f}_{body}\|$, where

$\Delta\|\boldsymbol{u}_{rms}\| \equiv \|\boldsymbol{u}_{rms}\|_{forced} - \|\boldsymbol{u}_{rms}\|_{unforced}$ and $\kappa \equiv \rho_\infty f^+$, showing higher amplification of $\Gamma = 9.4$ using the forcing mode from the original resolvent analysis, compared to $\Gamma = 7.0$ using that from the windowed analysis. The higher amplification agrees with the higher gain at $St = 0.06$ obtained from the original resolvent analysis (see figure 4), which measures the global response to the forcing input. Although the use of the windowed resolvent forcing profile shows lower amplification, the shock oscillation coupled with the shear layer fluctuation at the shock foot is more energetic, as observed in figure 7(*d*). These results validate the insights gained from resolvent analysis. Perturbations at the foot of the standing shock becomes amplified through the linear dynamics about the base flow to oscillate the shock in a violent manner, even at a Reynolds number that is commonly not associated with buffet.

4. Conclusions

We examined the origin of two-dimensional transonic buffet over a NACA 0012 airfoil at a Reynolds number of 2000 through resolvent analysis. While the transonic base state at this Reynolds number exhibits unsteadiness only due to the von Kármán shedding, we show that the amplification mechanism for buffet is present in the global dynamics. The response and forcing modes from the windowed resolvent analysis revealed that the source of transonic buffet lies at the shock foot. Perturbations within the boundary layer at the shock foot can be amplified to produce oscillations about the standing shock over the airfoil with a low frequency of $St = 0.06$. We also noted that such perturbations are closely tied to the change in the flow around the trailing edge, suggesting the effectiveness of trailing-edge buffet control devices. The identified buffet mechanism was validated by companion DNS that generated buffet by perturbing the flow through the forcing modes. The results show that even at a Reynolds number much lower than what is traditionally associated with transonic buffet, we are able to instigate buffet through the hidden amplification mechanisms. This mechanism does not require the flow to be at high Reynolds number. The findings from the present study offers fundamental insights not only into the origin of buffet but also for low-Reynolds-number compressible aerodynamics with the growing interest in the development of Martian aircraft.

Acknowledgements

Y.K. and M.K. gratefully acknowledge the Overseas Travel Assistance Program supported by the TUAT President's Office. C.-A.Y. and K.T. gratefully acknowledge support from the US Office of Naval Research (Program Manager: Dr B. Holm-Hansen, grant no. N00014-19-1-2460) and the US Air Force Office of Scientific Research (Program Managers: Drs G. Abate and D. Smith, grant no. FA9550-18-1-0040).

Declaration of interests

The authors report no conflict of interest.

References

ANYOJI, M., NUMATA, D., NAGAI, H. & ASAI, K. 2015 Effects of Mach number and specific heat ratio on low-Reynolds-number airfoil flows. *AIAA J.* **53** (6), 1640–1654.

BRÈS, G. A., HAM, F. E., NICHOLS, J. W. & LELE, S. K. 2017 Unstructured large-eddy simulations of supersonic jets. *AIAA J.* **55** (4), 1164–1184.

CROUCH, J. D., GARBARUK, A., MAGIDOV, D. & TRAVIN, A. 2009 Origin of transonic buffet on aerofoils. *J. Fluid Mech.* **628**, 357–369.

DANDOIS, J. 2016 Experimental study of transonic buffet phenomenon on a 3D swept wing. *Phys. Fluids* **28** (1), 016101.

DECK, S. 2005 Numerical simulation of transonic buffet over a supercritical airfoil. *AIAA J.* **43** (7), 1556–1566.

DELERY, J. M. 1985 Shock wave/turbulent boundary layer interaction and its control. *Prog. Aerosp. Sci.* **22** (4), 209–280.

FREUND, J. B. 1997 Proposed inflow/outflow boundary condition for direct computation of aerodynamic sound. *AIAA J.* **35** (4), 740–742.

FUKUSHIMA, Y. & KAWAI, S. 2018 Wall-modeled large-eddy simulation of transonic airfoil buffet at high Reynolds number. *AIAA J.* **56** (6), 2372–2388.

GAO, C., ZHANG, W., KOU, J., LIU, Y. & YE, Z. 2017 Active control of transonic buffet flow. *J. Fluid Mech.* **824**, 312–351.

GIANNELIS, N. F., VIO, G. A. & LEVINSKI, O. 2017 A review of recent developments in the understanding of transonic shock buffet. *Prog. Aerosp. Sci.* **92**, 39–84.

GROSSI, F., BRAZA, M. & HOARAU, Y. 2014 Prediction of transonic buffet by delayed detached-eddy simulation. *AIAA J.* **52** (10), 2300–2312.

IOVNOVICH, M. & RAVEH, D. E. 2012 Reynolds-averaged Navier–Stokes study of the shock-buffet instability mechanism. *AIAA J.* **50** (4), 880–890.

IOVNOVICH, M. & RAVEH, D. E. 2015 Numerical study of shock buffet on three-dimensional wings. *AIAA J.* **53** (2), 449–463.

JACQUIN, L., MOLTON, P., DECK, S., MAURY, B. & SOULEVANT, D. 2009 Experimental study of shock oscillation over a transonic supercritical profile. *AIAA J.* **47** (9), 1985–1994.

JEUN, J., NICHOLS, J. W. & JOVANOVIĆ, M. R. 2016 Input–output analysis of high-speed axisymmetric isothermal jet noise. *Phys. Fluids* **28** (4), 047101.

JOVANOVIĆ, M. R. 2004 Modeling, analysis, and control of spatially distributed systems. PhD thesis, University of California, Santa Barbara, CA.

JOVANOVIĆ, M. R. & BAMIEH, B. 2005 Componentwise energy amplification in channel flows. *J. Fluid Mech.* **534**, 145–183.

KONING, W. J. F., JOHNSON, W. & GRIP, H. F. 2019 Improved Mars helicopter aerodynamic rotor model for comprehensive analyses. *AIAA J.* **57** (9), 3969–3979.

LEE, B. H. K. 2001 Self-sustained shock oscillations on airfoils at transonic speeds. *Prog. Aerosp. Sci.* **37** (2), 147–196.

LEVY, L. L. 1978 Experimental and computational steady and unsteady transonic flows about a thick airfoil. *AIAA J.* **16** (6), 564–572.

MCCORMICK, D. C. 1993 Shock/boundary-layer interaction control with vortex generators and passive cavity. *AIAA J.* **31** (1), 91–96.

MCDEVITT, J. B. & OKUNO, A. F. 1985 Static and dynamic pressure measurements on a NACA 0012 airfoil in the Ames high Reynolds number facility. *NASA Tech. Rep.* TP-2485. National Aeronautics and Space Administration.

MCKEON, B. J. & SHARMA, A. S. 2010 A critical-layer framework for turbulent pipe flow. *J. Fluid Mech.* **658**, 336–382.

MUNDAY, P. M. & TAIRA, K. 2018 Effects of wall-normal and angular momentum injections in airfoil separation control. *AIAA J.* **56** (5), 1830–1842.

MUNDAY, P. M., TAIRA, K., SUWA, T., NUMATA, D. & ASAI, K. 2015 Nonlinear lift on a triangular airfoil in low-Reynolds-number compressible flow. *J. Aircraft* **52** (3), 924–931.

NITZSCHE, J. 2009 A numerical study on aerodynamic resonance in transonic seperated flow. In *International Forum on Aeroelasticity and Structural Dynamics, Seattle, WA*, IFASD Paper 2009-126.

OHMICHI, Y., ISHIDA, T. & HASHIMOTO, A. 2018 Modal decomposition analysis of three-dimensional transonic buffet phenomenon on a swept wing. *AIAA J.* **56** (10), 3938–3950.

SARTOR, F., METTOT, C. & SIPP, D. 2014 Stability, receptivity, and sensitivity analyses of buffeting transonic flow over a profile. *AIAA J.* **53** (7), 1980–1993.

SCHMIDT, O. T., TOWNE, A., RIGAS, G., COLONIUS, T. & BRÈS, G. A. 2018 Spectral analysis of jet turbulence. *J. Fluid Mech.* **855**, 953–982.

SEEGMILLER, H. L., MARVIN, J. G. & LEVY, L. L. JR 1978 Steady and unsteady transonic flow. *AIAA J.* **16** (12), 1262–1270.

SHI, J., HU, C. & SHU, C. W. 2002 A technique of treating negative weights in WENO schemes. *J. Comput. Phys.* **175** (1), 108–127.

TAIRA, K., BRUNTON, S. L., DAWSON, S. T. M., ROWLEY, C. W., COLONIUS, T., MCKEON, B. J., SCHMIDT, O. T., GORDEYEV, S., THEOFILIS, V. & UKEILEY, L. S. 2017 Modal analysis of fluid flows: an overview. *AIAA J.* **55** (12), 4013–4041.

TAIRA, K., HEMATI, M. S., BRUNTON, S. L., SUN, Y., DURAISAMY, K., BAGHERI, S., DAWSON, S. T. M. & YEH, C.-A. 2019 Modal analysis of fluid flows: applications and outlook. *AIAA J.* doi:10.2514/1.J058462.

TREFETHEN, L. N., TREFETHEN, A. E., REDDY, S. C. & DRISCOLL, T. A. 1993 Hydrodynamic stability without eigenvalues. *Science* **261** (5121), 578–584.

YEH, C.-A. & TAIRA, K. 2019 Resolvent-analysis-based design of airfoil separation control. *J. Fluid Mech.* **867**, 572–610.

ZHANG, W. & SAMTANEY, R. 2016 Biglobal linear stability analysis on low-*Re* flow past an airfoil at high angle of attack. *Phys. Fluids* **28** (4), 044105.